Skin depth at microwave frequencies of sea foam layers with vertical profile of void fraction

Magdalena D. Anguelova[1] and Peter W. Gaiser[1]

[1]   To develop a foam emissivity model, we started a systematic investigation of sea foam properties at microwave frequencies from 1 to 37 GHz. We first examined various permittivity formulae to find the most suitable one for obtaining the dielectric constant of sea foam. This paper presents an investigation of the skin depth of vertically structured foam layers for the first time. Various void fraction profiles representing variations of foam properties within the foam thickness are examined. The skin depth of foam layer thicknesses from 0.2 cm to 10 cm is obtained. The dependence of foam skin depth on frequency and foam layer thickness is investigated and compared to seawater skin depth. It was found that for exponential void fraction profile ranging from 99% at the air-foam interface to 1% at the foam-seawater boundary, the foam skin depth varies from 0.17 cm to no more than 7 cm. Possible variations of the foam skin depth due to permittivity formula choice, seawater temperature and salinity, and shape of void fraction profile, as well as its upper and lower limits, are presented. Analyses of the results help explain the sensitivity of microwave frequencies to foam layer thicknesses, infer the formation of the emissivity signal and its variations from foam-covered surfaces, infer implications for the passive remote sensing of whitecaps, discuss modeling approaches for vertically structured foam layers, and infer qualitatively the relative contributions of different foam structures to the absorption and emission of electromagnetic radiation. These findings give conceptual understanding of foam emissivity.

1.   Introduction

[2]   Sea foam layers constitute the whitecaps created when wind waves break in the open ocean. Whitecaps are involved in climate change through various air-sea interaction processes [*Andreas et al.*, 2008; *Wanninkhof et al.*, 2009; *de Leeuw et al.*, 2011] and affect the accuracy of geophysical retrieval algorithms [*Gordon and Wang*, 1994; *Yueh*, 1997; *Camps et al.*, 2005; *Padmanabhan et al.*, 2006]. To account for sea foam effects in climate models and geophysical retrievals, it is desirable to reliably observe and model the fraction of the ocean surface covered with foam (whitecap fraction). Estimates of whitecap fraction from microwave satellite measurements require a model for foam emissivity e_f [*Pandey and Kakar*, 1982; *Wentz*, 1983; *Anguelova and Webster*, 2006]. However, the knowledge of sea foam dielectric and radiative properties necessary for the modeling of e_f at microwave frequencies from 1 to 37 GHz, a range of frequencies measured by most of the operating and upcoming satellite-borne radiometers, is currently incomplete. The

purpose of this paper is to expand our knowledge of foam dielectric properties and thereby contribute to the modeling of foam emissivity.

[3] Generally, basis for the dielectric properties of a medium is its relative dielectric constant (permittivity). Permittivity determines such intrinsic characteristics of the medium as skin (and penetration) depth, impedance, refractive index, etc. These quantities control the attenuation due to absorption and scattering and the transmission and reflection of the electromagnetic (EM) radiation in the medium. These radiative processes affect, in turn, the energy lost in and then emitted by the medium. Therefore, understanding of the relative importance of all these characteristics and processes can assist the choice of an approach to model e_f, the formulation of relevant assumptions and/or simplifications, and the interpretation of the model results.

[4] With this in mind, we started a detailed examination of the basic dielectric properties of sea foam with a study investigating how to predict the complex permittivity ε_f of sea foam with currently available information [*Anguelova*, 2008]. The present paper continues this investigation by focusing on the foam skin depth. We conclude this series of papers with considerations of the foam properties affecting the propagation of the EM radiation through foam (M. D. Anguelova and P. W. Gaiser, Dielectric and radiative

---

[1]Remote Sensing Division, Naval Research Laboratory, Washington, DC, USA.

properties of sea foam at microwave frequencies: Conceptual understanding of the high emissivity of foam, submitted to *Remote Sensing*, 2011, hereinafter referred to as AG11).

[5] In this study, we pursue two specific goals: (1) investigate how best to model the vertical profile of foam mechanical structure and dielectric properties and (2) obtain and analyze the skin depth of vertically structured layers of sea foam to gain physical understating of the emissivity of sea foam. After a survey of background information relevant to this study (section 2), we present various profiles for the vertical structure of foam layers and foam skin depth for various conditions (section 3). Analyses of these results (section 4) help explain the sensitivity of microwave frequencies to foam layer thicknesses, deduce the variation of the emissivity from foam-covered surfaces, discuss modeling approaches for vertically structured foam layers, and infer qualitatively the relative contributions of different foam structures to the absorption and emission of EM radiation. Our findings add to the conceptual understanding of foam emissivity and thus to the physical basis on which to model it.

2. Background

2.1. Sea Foam as a Medium

[6] From an oceanographic point of view, the term "sea foam" involves both whitecaps on the surface and bubble plumes below. The whitecaps on the surface are further distinguished as active and residual foam associated with different stages of the whitecap lifetime, either the initial moment of wave breaking or the decay of bubble plumes, respectively (see *Anguelova* [2008, section 2.1] for an extended definition of sea foam). For microwave remote sensing applications, we are concerned with the surface foam layers, thick and thin depending on their lifetime stage (active and residual), and the dense bubbly mixture immediately below, excluding deeper bubble plumes.

[7] A review of laboratory and field experiments [*Anguelova*, 2008, section 2.2] helps to establish the specific physical structure of sea foam within a surface foam layer: large thin-walled bubbles close to the air-foam interface characterized by high air content (dry foam); and smaller, thick-walled bubbles with high water content (wet foam) close to the seawater boundary. Bubble dimensions and size distribution describe this foam structure in microscopic terms. Foam void fraction f_a (defined as the fraction of a unit volume of seawater that is occupied by air) and foam layer thickness t are the foam macroscopic characteristics. An alternative quantity that can characterize a vertically stratified foam layer by connecting its characteristics $f_a(z)$ and t is the total amount of seawater (seawater column) $Q_t(z) = \int_0^t [1 - f_a(z)]dz$ which this layer can hold.

2.2. Definition of Skin Depth

[8] Basic physical relationships from electromagnetic theory have been used in this study. The foam penetration depth δ is [*Ulaby et al.*, 1982, p. 847]:

$$\int_0^\delta k_a(z)dz = 1, \qquad (1a)$$

where $k_a(z)$ is the power absorption coefficient involving the complex dielectric constant of sea foam $\varepsilon_f(z)$ via the electric field attenuation coefficient α, $k_a(z) = 2\alpha = 2.\frac{2\pi F}{c}.\left|\mathrm{Im}\sqrt{\varepsilon_f(z)}\right|$, with c the speed of light and F the frequency in Hz. For foam skin depth d, equation (1a) changes to:

$$\int_0^d \alpha(z)dz = 1, \qquad (1b)$$

[9] Only the absorption coefficient $k_a(z)$ contributes to equations (1a) and (1b). The contribution of the scattering coefficient $k_s(z)$ to the total attenuation (extinction) in sea foam $k_e(z) = k_a(z) + k_s(z)$ is not considered because scattering is weak to negligible in sea foam [*Anguelova*, 2008, section 2.3]. When $\varepsilon_f(z)$ is constant in foam depth z, equations (1a) and (1b) give

$$\delta = \frac{1}{2\alpha} = \frac{1}{2}\left[\frac{2\pi F}{c}.\left|\mathrm{Im}\sqrt{\varepsilon_f}\right|\right]^{-1} \qquad (2a)$$

$$d = \frac{1}{\alpha} = 2\delta. \qquad (2b)$$

[10] The difference between δ and d is their definition, respectively, as the *e*-folding attenuation of the energy flux transported by EM radiation and as the reduction of the electric field amplitude to e^{-2} [*Maul*, 1985, p. 419]. Therefore, the skin depth d is the medium thickness over which the propagating EM radiation decreases by 86% from its initial value, i.e., $1 - e^{-2}$ [*Ulaby et al.*, 1986, p. 1420].

2.3. Sea Foam Permittivity

[11] To obtain the foam skin depth, we need the complex dielectric constant of sea foam $\varepsilon_f = \varepsilon'_f - i\varepsilon''_f$. *Anguelova* [2008] investigated the applicability of various formulae (i.e., mixing rules) for computing ε_f at microwave frequencies from 1 to 37 GHz. In this study we use the Polder-van Santen (PS) mixing rule:

$$\frac{\varepsilon_f - \varepsilon}{\varepsilon_f + 2\varepsilon + 2(\varepsilon_f - \varepsilon)} = f_a\frac{1 - \varepsilon}{1 + 2\varepsilon + 2(\varepsilon_f - \varepsilon)}. \qquad (3)$$

Equation (3) is identical to the generalized mixing rule given by *Sihvola* [1999, equation (9.7)], but it is written in notations appropriate for foam, i.e., the seawater, with complex dielectric constant ε, is assigned as an environment and air bubbles as inclusions with volume fraction f_a. Re-arranging equation (3), one obtains the quadratic equation representing the PS mixing rule in foam notations as given in *Anguelova* [2008, Table 1]. For most f_a values, the PS formula provides lower values for ε_f than those obtained with other mixing rules [*Anguelova*, 2008, section 3.4]. Using the PS formula in this study, we obtain an upper limit of foam skin depth in terms of dielectric constant; section 3.3 investigates variations of d due to various choices of mixing rule.

[12] We calculate ε with a double Debye model [*Stogryn*, 1997]. Table 1 lists the real and imaginary parts ε' and ε'' of

Table 1. Seawater Characteristics and Results for Foam Layers[a]

| | | | | Foam Skin Depth d (cm) for Various Foam Layer Thicknesses t (cm) | | | | | | |
F GHz	Re$\{\varepsilon\}$	Im$\{\varepsilon\}$	d_s (cm)	0.2	0.5	1.0	3.0	10.0	t_n (cm)	$Q_t(t_n)$ (cm)
1.4	**70.43**	**65.06**	**0.955**	0.62	1.01	1.47	2.82	6.45	2.15	0.9551
6.8	**62.53**	**34.14**	**0.336**	0.38	0.63	0.96	2.01	5.08	0.76	0.3357
10.7	**53.52**	**36.73**	**0.187**	0.29	0.50	0.78	1.73	4.52	0.42	0.1868
18.7	**36.60**	**37.21**	**0.091**	0.21	0.39	0.63	1.47	3.84	0.21	0.0910
23.8	**28.98**	**35.00**	**0.070**	0.19	0.35	0.59	1.37	3.54	0.16	0.0700
37.0	**17.79**	**28.03**	**0.046**	0.17	0.31	0.52	1.20	2.95	0.10	0.0461

[a]Seawater permittivity, ε (Re and Im parts), and corresponding skin depth, d_s, at the considered frequencies, F, and fixed water temperature (20°C) and salinity (34 psu) (bold text). Foam skin depth, d, for various frequencies, F, and foam layer thicknesses, t, computed using Polder-van Santen (PS) mixing rule for foam dielectric constant, ε_f, and exponential void fraction profile, $f_a(z)$ (Table 2, $m = 1$), with void fractions at the foam-air $v_{af} = 99\%$ and foam-water $v_{fw} = 1\%$ boundaries. Nominal foam layer thickness, t_n, and corresponding total amount of seawater contained in it, $Q_t(t_n)$ (section 4.1.2).

ε for the considered frequencies at water temperature $T_s = 20°C$ and salinity $S = 34$ psu; unless otherwise noted, these are used in all results (section 3) and analyses (section 4). Section 3.3 investigates variations of d due to variations of T_s and S. Figure 1 gives a plot of ε'_f and ε''_f as a function of f_a (Figures 1a and 1b) and frequency F (Figure 1c).

2.4. Survey of Void Fraction Profiles

[13] The vertical void fraction profile $f_a(z)$ of a foam layer is the principal cause for the variations of ε_f with depth z, $\varepsilon_f(z)$. We thus need to consider what vertical profile can plausibly represent $f_a(z)$ in foam layers. A survey of published results on both surface foam layers and deeper bubble plumes helps to establish possible vertical profiles.

[14] There are few measurements of foam void fraction close to the surface, and the reported results differ widely among them. On the one hand, *Bordonskiy et al.* [1978, Figure 1b], building on the experimental results of *Militskii et al.* [1977], present a profile of water content $Q_t(z)$ ($c(h)$ in authors' notation) measured in 1.5 cm thick foam layers in fresh water; its respective void fraction $f_a(z) = 1 - Q_t(z)$ decreases slowly from its large value at the air-foam interface (remaining almost constant for about 1 cm) initially, and decreases faster only in the last few millimeters above the foam-water interface. On the other hand, *Camps et al.* [2005, Figures 5 and 9] show a void fraction profile decreasing monotonically with depth. *Camps et al.* [2005] profiles are measured in fresh and diluted natural seawater over 8 cm depth, which includes a surface layer and dense bubbly mixture below it. As expected, the main change in the void fraction is in the surface foam layer of thickness about 1–1.4 cm, comparable to the layers which *Bordonskiy et al.* [1978] investigated. Because *Camps et al.* [2005] show profiles for fresh and salt water with similar shapes, we dismiss the possibility that the differences in the shape of the reported void fraction profiles are due to salinity. The most probable reason is how the foam was created: commercial shampoo in the *Militskii et al.* [1977] experiment versus a network of air diffusers with adjustable airflow in the *Camps et al.* [2005] experiment.

[15] The vertical distribution of bubble population $N(z)$ in bubble plumes has been extensively measured. It has been established that power [*Kolovayev*, 1976] or exponential [*Wu*, 1994] laws express the decrease of bubble population with depth. A functional dependence of $f_a(z)$ similar to that obtained from bubble plumes $N(z)$ is plausible because void

fraction can be evaluated from bubble population. Assuming that the same dependence is preserved on different scales, from a few meters for bubble plumes to a few centimeters for foam layers, we can consider exponential and power laws for void fraction profiles.

[16] Besides these measured profiles, various dielectric constant profiles have been assumed in models. *Webster et al.* [1976, p. 3096] and *Wilheit* [1979] assumed a linear transition of the refractive index of foam ($= \sqrt{\varepsilon_f}$) from that of the seawater value to that of the air. *Wilheit* [1978a] considered a combination of constant and linear transition parts to model dielectric changes due to changes in soil moisture with depth. *Raizer and Sharkov* [1982] opted for the hyperbolic tangent function to represent variations of dielectric properties in thin foam layers and for linear change of bubble radii in thick foam layers. *Raizer* [2007] uses the hyperbolic tangent formulation for the void fraction profile directly.

[17] In summary, we have identified a number of void fraction profiles whose suitability for foam layers should be evaluated, namely constant, linear, exponential, power law (more specifically quadratic, following *Kolovayev* [1976]), hyperbolic tangent, and a combination of constant and transitional parts.

[18] *Anguelova* [2008, section 2.4] suggested using the full range of void fractions in foam layers, from 1 at the air-foam interface to 0 at the foam-water boundary. The physical justification for this is to be able to model the emissivity of whitecaps in various lifetime stages, from foam on the crests of actively breaking waves to residual foam patches, and under various environmental conditions. With a survey of published results, *Anguelova* [2008] showed that, though void fraction values as high as 90–95% were anticipated [e.g., *Lamarre and Melville*, 1991] and used in models [e.g., *Droppleman*, 1970], void fractions greater than 65% were not observed [*Gemmrich and Farmer*, 1999]. Only recently, with new measurement techniques, void fractions up to 95–99% were documented during the active breaking of water waves [*Blenkinsopp and Chaplin*, 2007; *Ryu and Chang*, 2008]. These new measurements lend experimental support to the conclusion to use the full range of void fractions in sea foam. This full range of void fraction values is almost entirely included within the foam layer thickness t whatever it is, as published photographs [*Peltzer and Griffin*, 1987, Figure 6b; *Camps et al.*, 2005, Figure 5] or graphs [*Bordonskiy et al.*, 1978, Figure 1; *Camps et al.*, 2005, Figure 9] show.
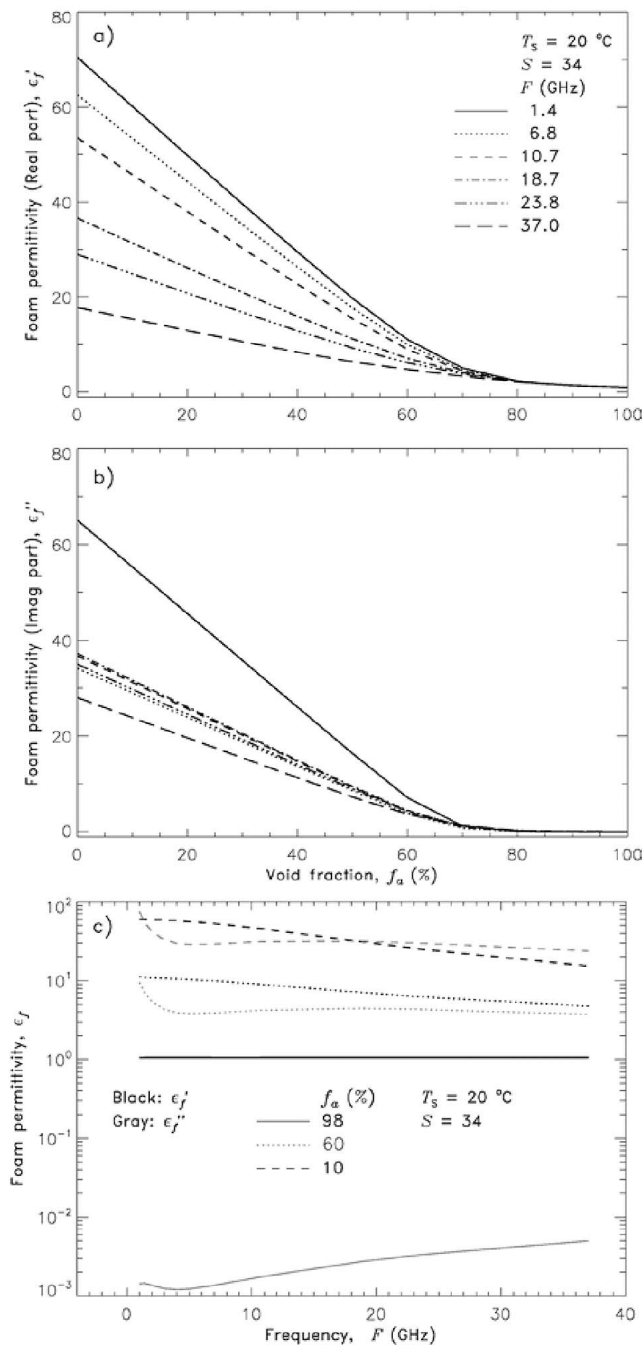
Figure 1. Foam dielectric constant (permittivity) at fixed seawater temperature ($T_s = 20°C$) and salinity ($S = 34$ psu): as a function of foam void fraction at various frequencies (a) real part $Re\{\varepsilon_f\} = \varepsilon_f'$; (b) imaginary part $Im\{\varepsilon_f\} = \varepsilon_f''$; and (c) as a function of frequency at foam void fractions representing dry foam ($f_a = 98\%$), wet foam ($f_a = 10\%$) and intermediate stage foam ($f_a = 60\%$).

2.5. Survey of Foam Layer Thicknesses

[19] Because we investigate changes in foam properties as a function of depth in foam layers, here we establish probable thicknesses of sea foam layers in the open ocean.

[20] We do not know with certainty what typical foam layer thicknesses are encountered in the ocean because data

on the thickness of the foamy rafts floating on the ocean surface are scarce. Moreover, most of the reported thicknesses of foam layers are for artificially created foam, not natural. This is a problem because artificial seawater, which has different chemical composition (especially the organic compounds), forms thinner foam layers than those of natural seawater [*Bikerman*, 1953, p. 53]. Meanwhile, there is a wealth of data on the entrainment depth of deeper bubble plumes; some among many are *Thorpe* [1982], *Walsh and Mulhearn* [1987], *Wu* [1994], *Melville et al.* [1995], and *Dahl and Jessup* [1995]. Thus, once again, a survey of measurements of both surface foam layers and deeper bubble plumes helps to identify a range of expected values for foam layer thickness t.

[21] *Williams* [1971] measured the emissivity of foam, stabilized with a small amount of detergent, in layers with various thicknesses, from single-layer bubble rafts with thickness of $O(1$ mm$)$ to multiple layers with overall t from 0.2 cm up to 12 cm. Using "commercial shampoo with different biological and chemical detergents," *Militskii et al.* [1977] created and examined foam layers with thickness of 1–1.5 cm. Investigating the stability of foam layers in seawater purified as much as possible by removing surface-active material, *Peltzer and Griffin* [1988] worked with foam layers with heights up to 9 cm. They observed decaying layers with thicknesses less than 0.5 cm. *Reising et al.* [2002] report a foam thickness distribution obtained during experiments at Naval Research Laboratory Chesapeake Bay Detachment [*Rose et al.*, 2002]. Though the foam was created artificially (with a foam generator consisting of gas-permeable tubes suspended below the water surface), the water composition was certainly closer to natural seawater than those used in the laboratory experiments cited above. The observed thicknesses range from 0.5 cm to 4 cm with a pronounced peak around 3.3 cm and a smaller one at 1.3 cm. *Camps et al.* [2005] show vertical profiles of foam and void fraction created with air diffusers at various salinity values obtained from natural seawater mixed with river water. The surface foam layers seen in their figures are up to 2 cm thick.

[22] Acoustic measurements in lakes under various wind speeds show penetration depths of bubble clouds (plumes) down to a few meters [*Thorpe*, 1982]. *Gemmrich and Farmer* [1999], on the other hand, conclude from their field measurements at wind speeds up to 18 ms^{-1} that "98% of deep water breaking waves have shallow air entrainment," less than 20 cm. Comparisons of penetration depths of background bubble population [*Leifer et al.*, 2006, Table 1] and of bubble plumes below breaking waves [*Leifer and de Leeuw*, 2006, Table 1] observed in both laboratory and field experiments confirm that the penetration depths associated with breaking waves are shallower.

[23] On the basis of field measurements of bubble plume depths and laboratory measurements of foam layer thicknesses, it could be expected that in the ocean the foam thickness at the surface, not the bubble plumes, may range from at least 0.1 cm to more than 12 cm. Expecting such foam thicknesses is in general agreement with the model of *Reul and Chapron* [2003, section 6]. In the following, only for convenience of representing and discussing results, we impose an arbitrary division of these observable thicknesses at $t = 1$ cm to signify either newly formed active whitecaps or high-wind conditions (e.g., above 7 m s^{-1})

Table 2. Formulae for Various Void Fraction Profiles

Void Fraction Profile	Profile Formula $f_a(z)$, $z \geq 0$	Coefficient a_V From: $f_a(z) = v_{af}$ @z = 0	Coefficient b_V From: $f_a(z) = v_{fw}$ @z = t
Constant	$f_a(z) = a_V$	$a_V = v_{af}$	NA
Linear	$f_a(z) = a_V - b_V z$	$a_V = v_{af}$	$b_V = \frac{1}{t}(v_{af} - v_{fw})$
Quadratic (power)	$f_a(z) = a_V - b_V z^2$	$a_V = v_{af}$	$b_V = \frac{1}{t^2}(v_{af} - v_{fw})$
Exponential	$f_a(z) = a_V - m.e^{b_V z}$	$a_V = v_{af} + m$	$b_V = \frac{1}{t}.\ln\left(\frac{m + v_{af} - v_{fw}}{m}\right)$
Hyperbolic tan	$f_a(z) = \tanh^2[a_V.(1 - z.b_V)]$	$a_V = \mathrm{arctanh}(\sqrt{v_{af}}$	$b_V = \frac{1}{t}\left(1 - \frac{\mathrm{atanh}\left(\sqrt{v_{fw}}\right)}{\mathrm{atanh}\left(\sqrt{v_{af}}\right)}\right)$
Combined (Const+lin)	$f_a(z) = a_V - b_V z$	$a_V = \begin{cases} v_{af} & 0 \leq z \leq t_c \\ v_{af} + \frac{v_{af} - v_{fw}}{t - t_c} t_c & t_c \leq z \leq t \end{cases}$	$b_V = \begin{cases} 0 & 0 \leq z \leq t_c \\ \frac{v_{af} - v_{fw}}{t - t_c} & t_c \leq z \leq t \end{cases}$

when 1 cm $\leq t <$ 12 cm and decaying residual whitecaps or low-wind conditions when 0.1 cm $< t <$ 1 cm.

3. Results

3.1. Void Fraction Profile of a Foam Layer

[24] To encompass measured and assumed possibilities, we examine all identified void fraction profiles (section 2.4). Table 2 lists the equations representing constant, linear, quadratic, exponential, hyperbolic tangent, and combined f_a profiles. Coefficients a_V and b_V in the functional form for each profile are determined from the following boundary conditions:

$$f_a(z) = \begin{cases} v_{af} & @\, z = 0 \\ v_{fw} & @\, z = t \end{cases}, \qquad (4)$$

where v_{af} and v_{fw} are chosen values of the void fraction at the air-foam and foam-water boundaries. With a lower limit $v_{fw} = 1\%$, we attempt to include the surface foam layer entirely but exclude deeper, more rarefied bubble plumes.

[25] We can shape the void fraction profile as we desire by choosing a specific functional form and/or parameters in some of the profiles. This is illustrated in Figure 2a, which gives plots of the void fraction changes with depth $f_a(z)$ as modeled with the considered functional forms (Table 2) over the full range (from $v_{af} = 99\%$ to $v_{fw} = 1\%$) in a 5 cm thick foam layer. The constant profile is given for $f_a(z) = 95\%$. In the combined (constant+linear) profile, the connecting point t_c between the constant and transitional parts (see the formula in Table 2) is arbitrarily chosen to be at 2/3 of the layer thickness from the foam-air interface. The basis for this arbitrary choice is the slow change of the void fraction in the upper part of the foam layer reported in the work of *Bordonskiy et al.* [1978]. Changing parameter m in the exponential profile, we get profiles close to the linear one (e.g., at $m = 3$) or "push" it beyond the hyperbolic tangent and close to the combined profile with $m = 0.01$. Similar control of the shape of the hyperbolic tangent profile can be achieved if its coefficient a_V is chosen arbitrarily instead of determining it from the v_{af} value (see Table 2); its coefficient b_V is fixed as $b_V = 1/t$ so that $f_a(z) = \tanh^2[m.(1 - z/t)]$. In this case the choice of m determines the upper limit v_{af} while the lower limit v_{fw} is always 0.

[26] Figure 2b gives a plot of the total amount of seawater that different void fraction profiles contain as a function of foam layer thickness, $Q_t(t)$. The figure is a clear visualization of two intuitively expected results. One is, of course, that, for a specific $f_a(z)$ profile, the thicker the foam layer, the more seawater it holds. Another is the change of Q_t among the different profiles. The linear profile contains the most seawater, while the 95%-constant profile holds the least amount. All other $f_a(z)$ profiles are between these two limits. There is a systematic decrease in Q_t values as $f_a(z)$ approaches a shape characterized by a slow change in the upper part of the foam, a sign for presence of predominantly dry foam (Figure 2a). Variations of the upper and lower limits v_{af} and v_{fw} of a specific functional form produce f_a profiles with Q_t contents spread in a way similar to that shown in Figure 2b but over a wider range, up to Q_t of 10 cm.

[27] Following the findings of our survey of void fraction profiles (section 2.4), we re-scale the same range of f_a values (from v_{af} to v_{fw}) for various t by recalculating the coefficient b_V (and sometimes a_V, see Table 2) using equation (4). The re-scaling to various t preserves the shapes of all f_a profiles illustrated in Figure 2a for $t = 5$ cm. The change of the f_a range via v_{af} and v_{fw} in equation (4) also preserves the profile shapes with the one exception of the hyperbolic tangent profile. Unless otherwise noted, we illustrate our results (sections 3.2 and 3.3) and analyses (section 4) using an exponential $f_a(z)$ profile ($m = 1$, Table 2) with $v_{af} = 99\%$ and $v_{fw} = 1\%$. Section 4.4.1 discusses these choices.

3.2. Foam Skin Depth

[28] Penetration depth δ and skin depth d for foam layers with vertical profiles of the void fraction are obtained from equations (1a) and (1b) by finding the root of an equation of the form $F(x) = 0$ using an optimal Müller's method with the integration performed numerically with Simpson's rule [*Atkinson*, 1989]. Only the results for d are plotted and discussed here. For any frequency or layer thickness, the skin depth of vertically stratified foam is thicker than its corresponding penetration depth by a factor of 1.2 to 1.4. A factor of 2 between δ and d of vertically homogeneous media (equation (2b)) is thus an upper limit.
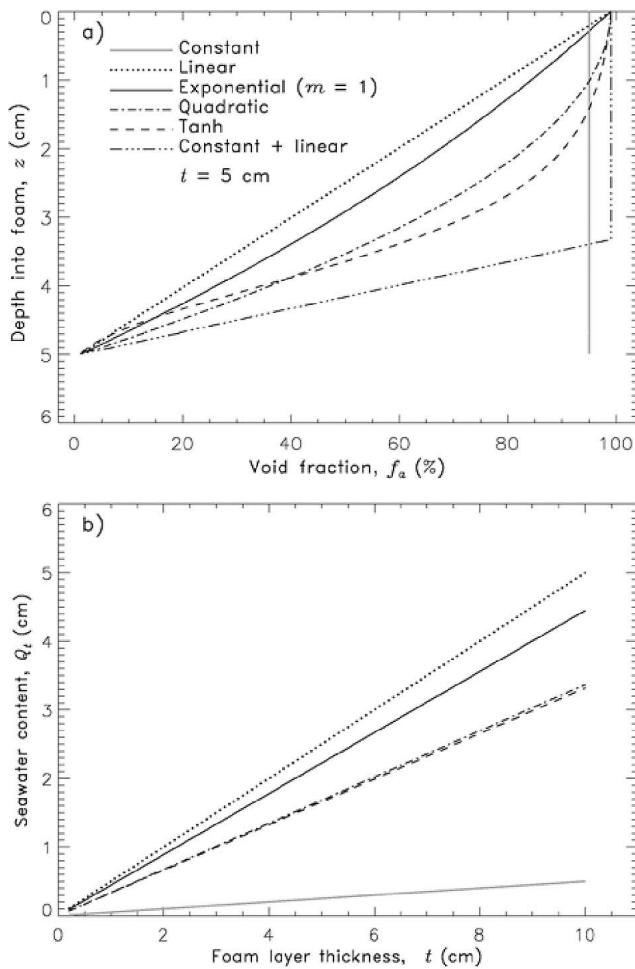
Figure 2. Void fraction profiles obtained with different functional forms (Table 2). (a) Void profiles in foam depth, $f_a(z)$, for a foam layer thickness $t = 5$ cm: constant (gray line, $f_a = 95\%$); linear (dotted line); exponential ($m = 1$, solid line); quadratic (dash-dot line); tangent hyperbolic (dashed line); combined profile (constant portion + linear transitional portion, dash-3dots line). (b) Total amount of seawater, Q_t, contained in different profiles as a function of foam layer thickness, t: linear (dotted line); exponential ($m = 1$, solid lines); quadratic (dash-dot line); tangent hyperbolic (dashed line); constant (gray line); combined not included.

[29] The skin depth d of sea foam obtained with equations (2a) and (2b) at fixed void fractions covering the full f_a range for all considered frequencies is shown in Figure 3. At any frequency, d is larger than the respective seawater skin depth d_s (the values at $f_a = 0$ for each F), by a factor of 1.1 at void fraction of 10% to a factor of 3.5 for f_a about 60%. The skin depth increases significantly as more air is mixed into the seawater to form foam and becomes thicker than 100 cm for any frequency when $f_a > 95\%$. This is expected because the presence of air diminishes the absorption by the air-seawater mixture, necessitating thicker foam skin depth in order to ensure an e-folding attenuation of the radiation in the foam skin depth.

[30] Figure 4 shows the frequency dependence of the foam skin depth $d(F)$ for foam layers with void fraction profile at
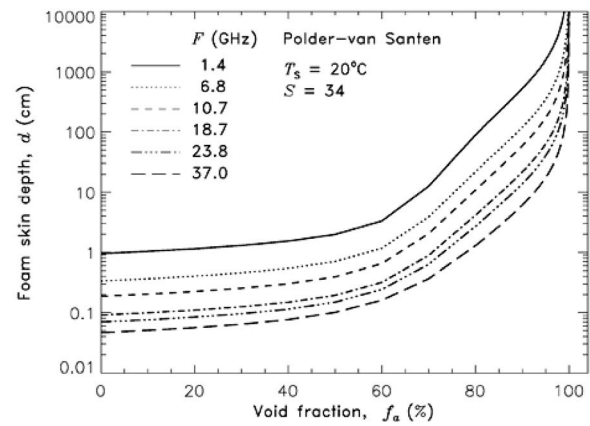

Figure 3. Foam skin depth, d, from Polder-van Santen mixing rule as a function of a range of specific void fraction values at fixed seawater temperature ($T_s = 20°C$) and salinity ($S = 34$ psu) for various frequencies (see the legend).

several foam layer thicknesses (Table 1). In contrast to d at fixed f_a values (Figure 3), the integral effect of the full $f_a(z)$ profile is to keep the values of d less than 7 cm, even at the lowest frequency ($F = 1.4$ GHz) and the thickest layer ($t = 10$ cm). A small yet perceptible change in the slopes of the curves at about 10 GHz (verified by the derivative $\partial d/\partial F$ and shown with a vertical line in Figure 4) marks two somewhat different behaviors of $d(F)$ at any foam thickness: small changes of d with frequency for $F > 10$ GHz and more significant variations of $d(F)$ for $F \leq 10$ GHz.

[31] Figure 4 shows that variations of foam layer thickness lead to large differences in the respective foam skin depths. Quantifying these differences as ratios, we find that generally d values may differ as little as by a factor of 1.4 and
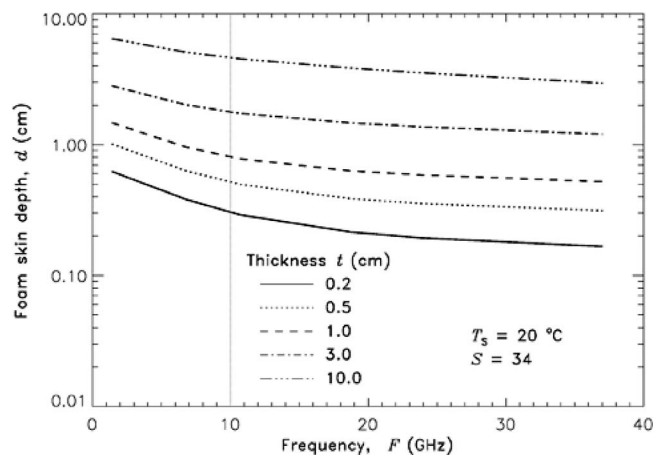

Figure 4. Foam skin depth as a function of frequency, $d(F)$, obtained using Polder-van Santen mixing rule with exponential void fraction profile ranging from 99% at the air-foam interface and 1% at the foam-seawater boundary at fixed seawater temperature ($T_s = 20°C$) and salinity ($S = 34$ psu) and foam layer thickness, t, as a parameter (see the legend in the figure). Vertical gray line at 10 GHz marks the point of slope change in $d(F)$ relationship (see section 3.2 for details).
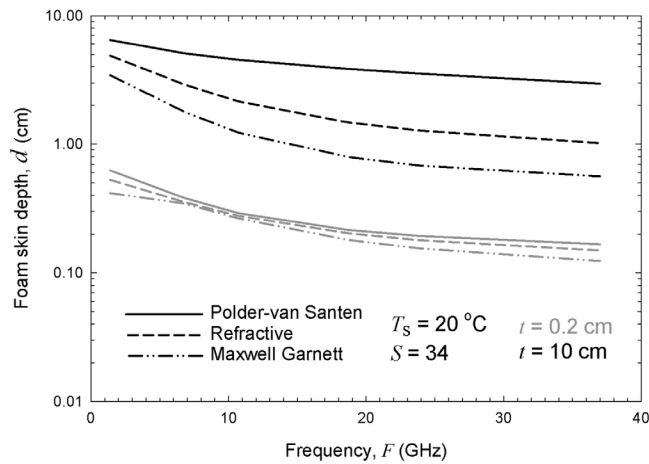
Figure 5. Frequency dependence of foam skin depth, $d(F)$, for three different choices of the mixing rule: Polder-van Santen (solid lines); refractive law (dashed lines); Maxwell-Garnett formula (dash-dot-dot lines). The group of gray lines is for foam layer thickness of $t = 0.2$ cm; black lines are for $t = 10$ cm.

up to a factor of about 20 at all frequencies. Heeding the association of foam thickness with either the lifetime stage of whitecaps or wind conditions (section 2.5), we infer that (1) the smallest differences in d could be associated either with low winds at any fixed stage of the whitecap lifetime or with foam thickness variations within residual foam; (2) differences within the same stage (active or residual) are smaller than those between stages at any specific wind speed; (3) d values are more affected by variations of t at higher frequencies (e.g., above 18 GHz) than at lower frequencies (e.g., 10 GHz and below).

3.3. Variations of Foam Skin Depth

[32] To investigate how other factors, besides t, affect foam skin depth, in the following we give the frequency dependence of foam skin depth $d(F)$ obtained with different parameters or at different conditions. All figures are plotted with the same scales as Figure 4 is, so that the variations can be compared to those associated with various foam layer thicknesses. While useful for comparisons, these scales are not optimal to reveal variations of d at some values of t. Thus, we do not use one t value consistently in all figures; rather, we illustrate the various cases using various t.

[33] Figure 5 presents $d(F)$ obtained with three different mixing rules for ε_f. Namely, the PS formula (equation (3), solid line), which gives an upper limit of d for a given dielectric constant (section 2.3); the Refractive mixing rule (Re) (dashed line), which was found to be the most suitable in representing sea foam [*Anguelova*, 2008]; and the Maxwell-Garnett (MG) formula (dash-dot-dot line), which defines the lower limit of d for a given dielectric constant. The gray lines are for foam layer thickness of 0.2 cm, and the group of black lines is for $t = 10$ cm. The influence of the mixing rule choice on the values of d is more pronounced for thick layers than for thin. Comparison to Figure 4 shows that at each frequency for a given t the range of changes between

the upper and lower values for d allowed by the mixing rules (PS and MG, respectively) is smaller than the changes caused by variations of foam layer thickness associated with active and residual whitecaps, e.g., 10 cm and 0.2 cm (section 2.5). However, the variations due to mixing rule choice for nearly all but the highest winds could be comparable to those due to t within the same whitecap life stage.

[34] Using a fixed mixing rule for ε_f (PS formula in our case, section 2.3), variations in d may occur due to dependence of ε_f on T_s and S [*Anguelova*, 2008]. At fixed salinity of 34 psu and foam thickness of 5 cm, changes of T_s from 0 to 30°C lead to changes in d values of 2.7 cm (Figure 6a); for $t = 0.2$ cm (not plotted), d varies by 0.6 cm over the T_s range. Salinity affects d at lower frequencies (Figure 6b), as expected [*Wilheit*, 1978b; *Anguelova*, 2008]. At fixed water temperature of 20°C and the same $t = 5$ cm, variations of salinity from 0 to 40 psu lead to changes in d of about 7.5 cm at a frequency of 1.4 GHz, but only 0.9 cm for frequencies from 6.8 to 37 GHz. For thinner foam layers, e.g., $t = 0.2$ cm, the variations of d have smaller absolute values, but the ratio between the d values at lower and higher frequencies remains the same as for thick layers, on the order of 10.

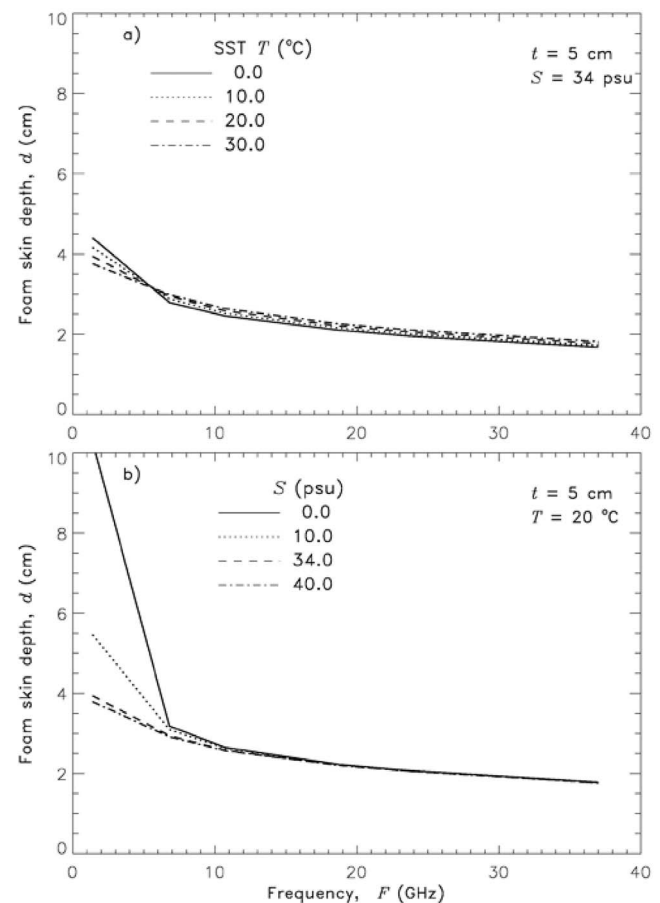[35] Figure 7 depicts changes in $d(F)$ for two foam layer thicknesses ($t = 0.2$ cm and $t = 10$ cm) due to choice

Figure 6. Frequency dependence of foam skin depth, $d(F)$, at fixed foam layer thickness of $t = 5$ cm and (a) fixed salinity ($S = 34$ psu) and various seawater temperatures; (b) fixed seawater temperature ($T_s = 20$°C) and various salinities.
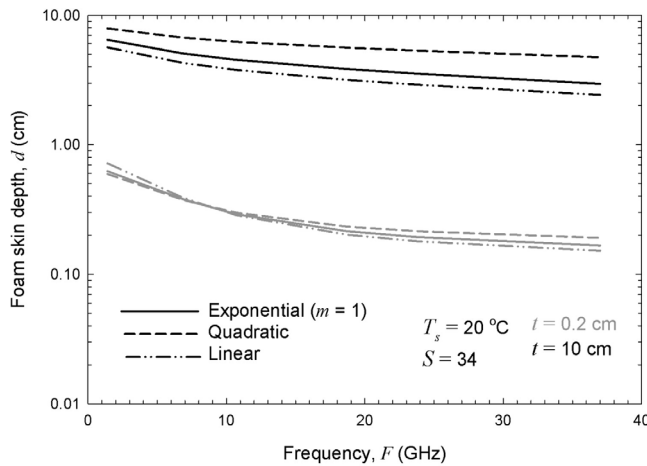
Figure 7. Frequency dependence of foam skin depth, $d(F)$, for three different void fraction profiles: exponential (solid lines); linear (dash-dot-dot lines); quadratic (dash lines). The group of gray lines is for foam layer thickness of $t = 0.2$ cm; black lines are for $t = 10$ cm.

of the void fraction profile (Table 2), namely exponential ($m = 1$, solid lines), quadratic (dashed lines) and linear (dash-dot-dot lines); for all three f_a profiles the upper and lower limits are $v_{af} = 99\%$ and $v_{fw} = 1\%$. The first observation from Figure 7 is that the linear f_a profile is associated with the lowest d values for most frequencies; only for low frequencies and $t = 0.2$ cm does it give larger d values. The less seawater the f_a profile contains (Figure 2b), the higher the d values are. By the same token, foam skin depths for hyperbolic tangent, combined, and constant profiles are all higher than the values for the quadratic one (not shown). Next, as in the case of mixing-rule effect, the overall variations of d are smaller for thinner (gray lines) than for thicker (black lines) foam layers. Finally, comparison of the results in Figure 7 to those in Figure 4 shows that at a specific foam thickness, the variations of d corresponding to various void fraction profiles are smaller than variations of d caused by a range of thicknesses.

[36] Figure 8 investigates the variations of $d(F)$ caused by changes of the upper and lower limits of the void fraction profile v_{af} (Figure 8a) and v_{fw} (Figure 8b) for $t = 1$ cm (marked with gray horizontal line); seawater skin depths are plotted for reference. When the lower limit of f_a is fixed at $v_{fw} = 1\%$ and the upper limit v_{af} varies from 99% to 10%, the foam skin depth decreases and approaches the corresponding values of d_s (Figure 8a). Figure 8b shows the converse situation. This time the upper limit is fixed at $v_{af} = 99\%$ and the lower limit v_{fw} varies from 1% to 90%. Accordingly, the foam skin depth increases. These observations hold for any other foam layer thickness t. Comparing Figure 8 to Figure 4, we see that changes in the range of the void fraction profile cause variations of d as wide as those due to variations of t from the thinnest to the thickest foam layer.

[37] Overall, most of the causes for foam skin depth variations—namely, mixing rule, seawater temperature, salinity, and the shape (i.e., functional form) of the void fraction profile—invoke changes in d in a range narrower than that due to variations of t. Changes in the upper and

lower limits of the void fraction profile lead to as wide variations in d as those caused by varying t.

4. Analysis

[38] The following sections present various analyses of our results (section 3) which help to gain physical understanding of the mechanisms of foam thermal emission and its variations, as well as the relative contributions of different foam structures to the attenuation of EM radiation. From this we infer useful implications for the remote sensing of whitecaps in different lifetime stages and under various environmental conditions and for the modeling of foam emissivity.

4.1. Bounds of Foam Skin Depth

[39] Analysis of the foam skin depth in relation to the seawater skin depth and the foam layer thickness reveals two important points in its frequency dependence $d(F)$.
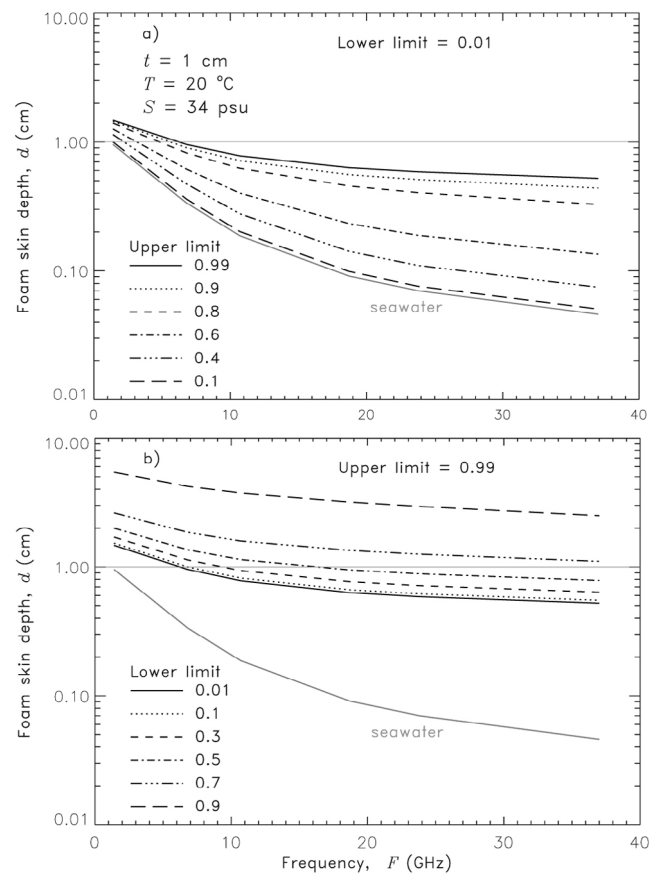

Figure 8. Frequency dependence of foam skin depth, $d(F)$, at fixed foam layer thickness of $t = 1$ cm and (a) lower limit of void fraction profile fixed at 1% and various upper limits (see the legend in the figure); (b) upper limit of void fraction profile fixed at 99% and various lower limits. Fixed seawater temperature ($T_s = 20°C$) and salinity ($S = 34$ psu). The skin depth of seawater (gray curves in both panels) is given for reference. Thin gray horizontal lines at $d = 1$ cm are drawn for better visualization of the differences between the two cases illustrated in the two panels.
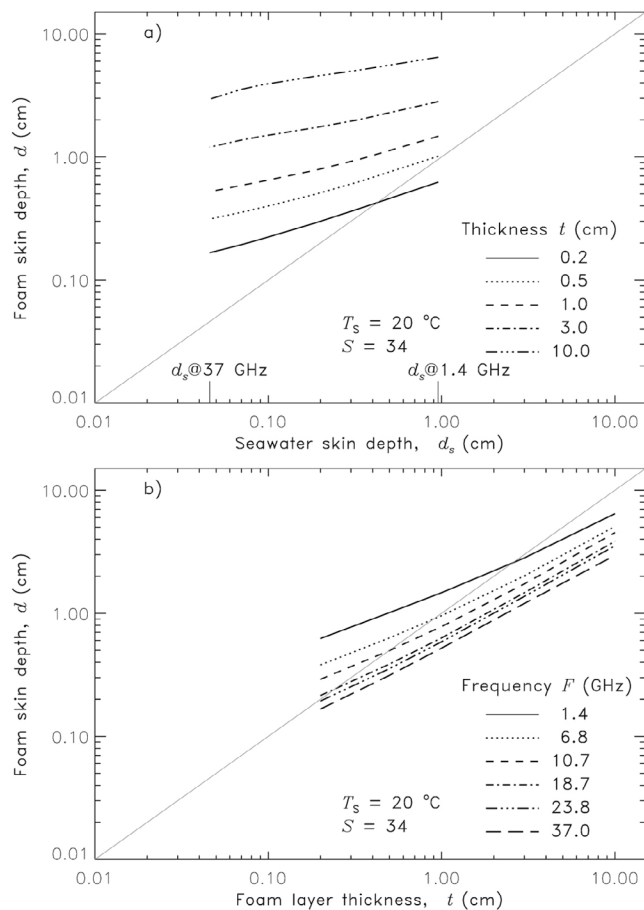
Figure 9. (a) Foam skin depth as a function of seawater skin depth, $d(d_s)$, for various foam layer thicknesses (see the legend in the figure). Gray line shows 1:1 relationship between d and d_s. d_s at 37 GHz and 1.4 GHz are marked on the x axis to assist the presentation in section 4.1.1. (b) Foam skin depth as a function of foam layer thickness, $d(t)$, for various frequencies (see the legend in the figure). Gray line shows 1:1 relationship between d and t. Both panels: Fixed seawater temperature $T_s = 20°C$ and salinity $S = 34$ psu.

4.1.1. Foam and Seawater Skin Depths

[40] When void fraction $f_a = 0$, foam transitions to seawater with $\varepsilon_f \equiv \varepsilon$ (Figure 1 and equation (3)) and then equation (1b) gives d_s at a given frequency. Because $\varepsilon_f < \varepsilon$ for any nonzero f_a value at any frequency (Figure 1), equation (1b) dictates that foam skin depth must be larger than seawater skin depth, $d > d_s$.

[41] Figure 9a shows d at each F for various t as a function of the corresponding d_s values (Table 1). The gray line in the figure denotes the 1:1 relationship between d and d_s. It is evident that the expected relationship $d > d_s$ holds at all frequencies for d values associated with $t \geq 0.5$ cm. For foam layers thinner than 0.5 cm, the figure suggests that a breach of the $d > d_s$ relationship would start to appear. Indeed, for $t = 0.2$ cm, foam skin depths become less than seawater skin depths ($d \leq d_s$) when $d_s \geq 0.42$ cm, which corresponds to frequencies ≤ 5.6 GHz. Because d_s is the ultimate lower limit in the foam-seawater system, reason-

able interpretation of the condition $d \leq d_s$ is that for probing frequencies below about 6 GHz foam layers thinner than 0.5 cm act as the seawater itself and their emissivity signals do not differ from that of the surrounding seawater.

[42] Such interpretation is supported by experimental observations which have also demonstrated restricted ability of low frequencies to probe thin foam layers. Measuring emissivity of foam with several thicknesses at multiple wavelengths (frequencies), *Bordonskiy et al.* [1978] reported for low frequencies (3.7 and 1.7 GHz) an increase of the emissivity over that of smooth water by 67% and 16%, respectively, from foam with thickness of 1 cm. However, the presence of 0.1 cm thick foam on the water surface did not change the emissivity at these frequencies; it remained as for foam-free water surface.

[43] In summary, the first important point in the frequency dependence of the foam skin depth is the point at which $d(F) \leq d_s(F)$ for a given t. This point marks the frequencies and foam layer thicknesses above which foam is distinguished from the surrounding seawater.

4.1.2. Foam Skin Depth and Foam Layer Thickness

[44] By virtue of its definition (section 2.2), skin depth is part of the medium and we can expect the relationship $d < t$ to hold. Figure 9b shows d as a function of t for each of the considered frequencies (Table 1). The 1:1 relationship between d and t (gray line) shows that for most of the considered frequencies F and observable values t the expected condition $d < t$ is fulfilled. However, it also demarcates cases for which a limit at $d = t$ is reached for some frequencies, followed by infraction of the expected relationship, i.e., $d > t$.

[45] Because Figure 9b compares dielectric (d) and mechanical (t) characteristics of the foam layer, it is clear that reaching a limit in the relationship between them charges t with more physical meaning than simply mechanical thickness. When d at a given frequency becomes equal to t, this means that the foam layer in its entirety provides the bulk (i.e., 86%) of the emissivity e_f emanated from the layer itself. Therefore, we can refer to this special foam layer thickness as "nominal thickness" and denote such cases with $t_n(F) = d(F)$.

[46] For a specific f_a profile, the nominal thickness at each frequency is unique. We can estimate $t_n(F)$ either directly from Figure 9b or using the total seawater content Q_t (section 2.1), a foam layer characteristic akin to d_s. Because to detect foam as such from its emissivity signal it is necessary that $d(F) > d_s(F)$ (section 4.1.1), the limiting relationship $t_n(F) = d(F)$ suggests that the nominal thickness is the thickness over which the specific f_a profile redistributes at least as much seawater as that contained in d_s, i.e., $Q_t(t_n) \approx d_s$. With this assumption, requiring $Q_t - d_s \leq 10^{-3}$, we find the nominal thicknesses $t_n(F)$ (Table 1) for the f_a profile illustrated in Figure 9b (see the end of section 3.1).

[47] In summary, the second important point in the frequency dependence of the foam skin depth is the point at which $d(F) = t \equiv t_n(F)$ for a specific f_a profile. This point marks the combinations of t and f_a which provide emission from the foam layer in its entirety.

4.2. Frequency Sensitivity to Foam Thickness

[48] Using the findings in section 4.1, here we gain insights on the mechanisms of thermal emission of foam-covered sea surface and its variations.

Table 3. Formation of Emissivity Signal at Different Frequencies From Foam Layers With Different Thicknesses[a]

| Foam Layers Forming e_f Signal | Relationship Between[b] | | | Contributions to e_f Signal | Variations of e_f Signal[c] |
	t and t_n	t and d	Q_t and d_s		
Radiometrically nominal	$t = t_n(F)$	$t = d(F)$	$Q_t(t) \approx d_s(F)$	Foam itself, entire t	Unique e_f for $t = t_n(F)$
Radiometrically thick	$t > t_n(F)$	$t > d(F)$	$Q_t(t) > d_s(F)$	Foam itself, part of t	Weak variation with t; Saturation for $t \gg t_n(F)$
Radiometrically thin	$t < t_n(F)$	$t < d(F)$	$Q_t(t) < d_s(F)$	Foam and seawater	Varies more with t; Seawater-like for $t \ll t_n(F)$

[a]The variables are as follows: frequency F; foam emissivity e_f; foam layer thickness t; nominal foam layer thickness for a given frequency $t_n(F)$; foam skin depth at a given frequency $d(F)$; total seawater content in a foam layer with a given thickness $Q_t(t)$; seawater skin depth for a given frequency $d_s(F)$.
[b]All entries are for exponential profile of foam void fraction f_a over the full range, from 99% at the air-foam boundary to 1% at the foam-water boundary.
[c]At fixed F and varying t.

4.2.1. Thermal Emission of Foam-Covered Sea Surface

[49] The interplay between foam skin depth d and foam layer thickness t leads to three possible ways of forming the thermal emission from a foam-covered sea surface (hereinafter referred to as "emissivity regimes"). The first emissivity regime is associated with foam layers which have thicknesses equal to their nominal thicknesses at a given frequency, $t \equiv t_n(F)$. Knowing the physical meaning of $t_n(F)$ (section 4.1.2), we refer to foam layers for which $t \equiv t_n(F) = d(F)$ and $Q_t(t) \equiv Q_t(t_n) \approx d_s(F)$ as "radiometrically nominal layers."

[50] The second emissivity regime is associated with foam layers thicker than the nominal thickness at a given frequency, $t > t_n(F)$. According to Figure 9b, $d(F) < t$ for such thicker foam layers; e.g., for 10.7 GHz (dashed line), d values are below the 1:1 (gray) line when t values are above the nominal thickness ($t_n = 0.42$ cm, Table 1) corresponding to the crossing point of the gray and dashed lines. The condition $d(F) < t$ means that only part of the foam would be enough to provide the same bulk (86%) of the emissivity signal; the thermal emission from the remaining parts of thicker layers would add little to the overall signal. In other words, the foam layer is thick enough to contain more than the minimally required seawater so that only a part of it suffices for e-folding attenuation. We refer to foam layers for which $t > d(F)$ and $Q_t(t) > d_s(F)$ as "radiometrically thick layers" in analogy to the term "optically thick layer" in aerosol studies.

[51] The third emissivity regime is associated with foam layers thinner than the nominal thickness at a given frequency, $t < t_n(F)$. For such thinner foam layers $t < d(F)$ (Figure 9b) and its physical meaning is that the foam layer itself is not enough to provide e-folding attenuation, i.e., it does not contain enough seawater, $Q_t(t) < d_s(F)$. Moreover, the condition $t < d(F)$ breaches the expected relationship $d < t$ (section 4.1.2). While $d < t$ is a binding requirement for solid objects—e.g., for a metal plate the well-defined physical thickness and interfaces render cases of $d > t$ not physical—we argue that infraction of the condition $d < t$ is conceivable for foam layers. *Williams*'s [1971] measurements of the emissivity of foam with different thicknesses over different substrates (metal and water) help realize that not just the foam itself, but the combination of foam floating on water is the system that determines the emissivity of a foam-covered water surface [*Anguelova*, 2008, section 2.3.1]. In such a system, $d > t$ may occur because the limited response of the foam layer (due to $Q_t(t) < d_s$) could be supported by the emitting potential of the seawater (or the bubble plume) below it. We refer to foam layers for which $t < d(F)$ and $Q_t(t) < d_s$ as "radiometrically thin layers."

[52] Table 3 summarizes the conditions for the different ways of forming an emissivity signal from a foam-covered surface.

4.2.2. Variations of Foam Emissivity Due to Foam Layer Thickness

[53] The way the thermal emission is formed in each emissivity regime determines characteristic variations of the emissivity signal e_f from foam layers with different thicknesses $e_f(t)$. Here we consider the $e_f(t)$ variations for a specific f_a profile, namely exponential f_a over the full range of void fraction values, from $v_{af} = 99\%$ to $v_{fw} = 1\%$ (see the end of section 3.1).

[54] For radiometrically nominal layers ($d = t_n$), each $t_n(F)$ (Table 1) provides a unique e_f signal. The only variation of e_f comes from varying F.

[55] The thermal emission of radiometrically thick layers is confined to part of the foam thickness and thus utilizes only a part of the full f_a profile (e.g., the dry foam). The resulting e_f signal would thus vary weakly with t and would approach a saturation level when $t \gg t_n(F)$. For example, at 10.7 GHz, no matter what the foam thickness is, 1 cm or 3 cm or even 12 cm (section 2.5), as long as it is thicker than about 0.4 cm (Table 1 and Figure 9b), the e_f signals from all these thicknesses would differ by at most 14%. Considering the small value of d for 37 GHz, a saturated e_f signal would be expected for almost all foam thicknesses encountered in the ocean. Model results support the notion of emissivity saturation for very thick layers [*Guo et al.*, 2001; *Chen et al.*, 2003].

[56] The e_f signal resulting from radiometrically thin layers would vary with t for reasons different from those causing t-variations in radiometrically thick layers. Namely, when t is varied, different portions of the underlying bubble plume are necessary in order to boost the emission up to the bulk of 86%. The e_f signal would approach seawater-like behavior when $t \ll t_n(F)$. *Bordonskiy et al.* [1978] observations (mentioned in section 4.1.1) support the expectation of seawater-like emissivity from thin foam layers. Table 3 summarizes the expected variations of e_f for varying t and fixed f_a profile.

[57] Using the definitions and interpretations introduced until now, we see from Figure 9b that 1 cm thick foam layer would be radiometrically thick for all frequencies above 10.7 GHz, close to nominal for 6.8 GHz, and radiometrically thin for 1.4 GHz. This 1 cm thick foam layer would produce different emissivity signals at different frequencies because the relationships between $Q_t(t = 1$ cm$)$ and $d_s(F)$ would determine different relationships between $d(F)$ and $t = 1$ cm. Overall, different frequencies would perceive the same foam
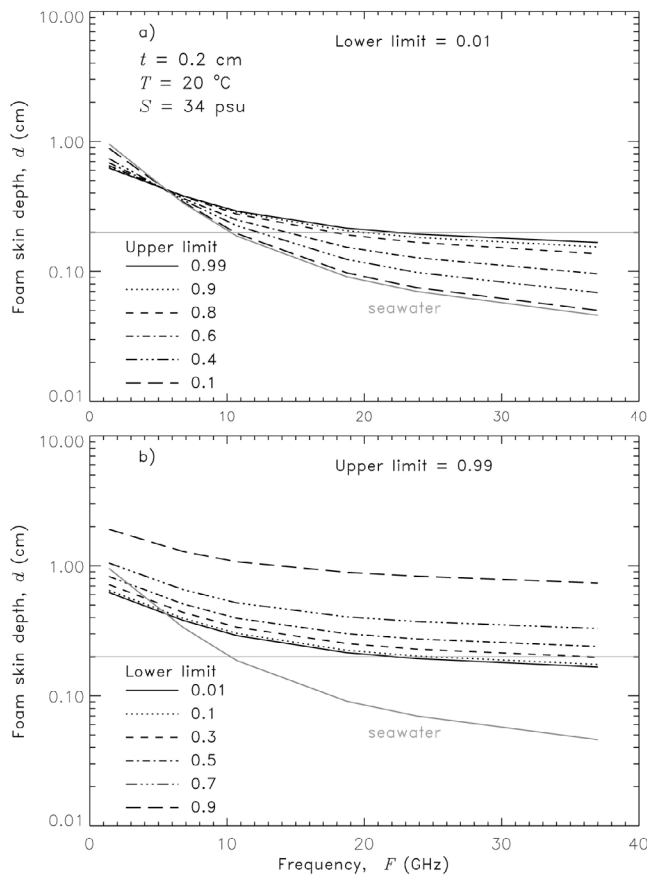
Figure 10. As Figure 8 but for foam layer thickness $t = 0.2$ cm.

layer differently. This constitutes the frequency sensitivity to foam thickness.

4.2.3. Variations of Foam Emissivity Due to Void Fraction Variations

[58] The variations of foam emissivity e_f for different combinations of frequency F and foam layer thickness t, inferred in section 4.2.2, are for the full range of the f_a profile. Here we investigate the impact of varying range of the f_a profile on e_f.

[59] A varied f_a range can affect e_f in two ways. One way is creating more possibilities for e_f variations within each emissivity regime. For radiometrically nominal foam layers ($d = t_n$), the number of unique pairs of t_n and corresponding e_f signal increases as varied upper and lower limits create an infinite number of possible f_a profiles. For radiometrically thick foam layers ($d < t_n$), the availability of different f_a ranges augments the anticipated weak $e_f(t)$ variations (Table 3). For radiometrically thin foam layers ($d > t_n$), more e_f variations would come from having more combinations of partial contributions from foam and seawater.

[60] Another way in which a varied f_a range affects e_f is to move the frequencies at which $d(F) = d_s(F)$ (section 4.1.1) and $d(F) = t_n(F)$ (section 4.1.2) thus shifting the frequency ranges for which one or another emissivity regime determines e_f. We show this with Figure 10, which is the same as Figure 8 but for a foam layer with $t = 0.2$ cm. The presence

of more dry foam in the layer shifts the point at which $d \leq d_s$ toward lower frequencies. This point reaches $F \approx 1.8$ GHz for f_a profile ranging from 0.6 to 0.99, and is not reached for any of the considered frequencies when $v_{fw} > 70\%$ (Figure 10a). Meanwhile, the point of $d = t_n$ shifts toward higher frequencies. As a result, the overall effect of having more dry foam in the layer is to extend the range of frequencies in which this layer acts as radiometrically thin and its e_f signal is formed from both the foam layer and the underlying bubble plume.

[61] When increasingly more wet foam is included in the f_a profile (Figure 10b), the frequency at which $d \leq d_s$ changes little—from 5.6 GHz for the full f_a range to $F \approx 5.55$ GHz for f_a ranging from 1% to 90% and to $F \approx 5.9$ GHz for f_a from 1% to 40%. The point of $d = t_n$ moves toward lower frequencies. Such changes shrink the frequency range over which the layer is radiometrically thin and thus for more frequencies the e_f signal is due to the foam itself.

4.3. Implications for Remote Sensing of Whitecaps

[62] The understanding gained in section 4.2 has useful implications for the remote sensing of oceanic whitecaps.

[63] First, because most combinations of t and f_a ranges ensure that $d > d_s$ for the considered frequencies (1.4 to 37 GHz), any of the currently operating and upcoming microwave radiometers can detect foam under most of the conditions that might be encountered in the open ocean. Next, limiting d to the range of observed foam layer thicknesses (section 2.5) substantiates previous statements (section 2.1 and *Anguelova* [2008]) that microwave radiometry is suitable for remote sensing of the surface foam layers which represent the horizontal extent of (i.e., the area covered by) the whitecaps. That is, passive microwave remote sensing measures predominantly the surface expression of breaking waves.

[64] Furthermore, because foam thickness depends on the environmental conditions or the lifetime stage of the whitecaps (section 2.5), the limitation of the low frequencies to detect thin foam layers (e.g., below 0.5 cm) means that frequencies below about 6 GHz cannot detect either whitecaps created under low winds or decaying whitecaps. For such conditions, measurements at higher frequencies (e.g., above 18 GHz) would be more suitable. Under high winds or during the active waves breaking—both being conditions when thick foam layers form—a wide range of whitecaps (e.g., from 3 cm to more than 12 cm) would be successfully detected by all frequencies above 6 GHz. Moreover, under these conditions, relatively small differences would be expected in whitecap measurements at various frequencies because the generated foam layers are radiometrically thick with weakly varying emissivity signals (Table 3). Under conditions which create foam layers with thicknesses from 0.1 cm to 3 cm, we can expect wider variations between remotely measured whitecaps at frequencies above 6 GHz because all emissivity regimes are possible.

[65] While all three emissivity regimes contribute to the signal from a foam-covered surface, two of them provide a signal from the foam itself, those involving radiometrically nominal and radiometrically thick foam layers (Table 3). Variations of e_f due to the foam itself are not easily separated from those of radiometrically thin layers. For example,

both radiometrically thin and radiometrically thick foam layers produce seawater-like behavior (long-dashed lines in Figures 8a and 10a). In the former case such behavior is due to more contribution from bubble plumes formed below thinner or drier foam. In the latter case it is due to the wet foam itself. The difficulty of separating these two regimes is not important when detection of foam on the surface is sought. The signal produced by any emissivity regime would thus be useful and sufficient for this purpose.

[66] However, being able to identify the emissivity regime opens possibilities to measure and study more processes. One possibility is to extend the mere detection of foam presence on the sea surface to recognizing the active and decaying stages of the whitecaps. Another possibility is to use the concept of radiometrically nominal foam layers to develop a technique to determine foam layer thicknesses with microwave radiometry. Finally, well characterized e_f variations associated with radiometrically thin foam layers at lower frequencies (e.g., below 10 GHz) would allow probing the whitecap vertical extent represented by bubble plumes below the foam floating on the surface. If the void fraction of a bubble plume could be determined in this way, one might be able to identify either the conditions that created the bubble plume or the stage of its lifetime. To realize such possibilities, it would be necessary to build an extensive database of e_f measurements at various F and t with various f_a ranges. Efforts to compile such a database can start with systematic laboratory experiments and continue with field observations.

4.4. Modeling Vertically Stratified Foam Layers

[67] Section 3.3 showed that there are various modeling choices and/or parameters that can affect foam skin depth d, and thus the modeled foam emissivity e_f. The question remains whether we can identify the best parameter ranges and modeling approaches to predict plausibly the e_f variations.

4.4.1. Choices for the Void Fraction Profile

[68] Three choices need to be considered when modeling the void fraction profile, namely profile shape, profile range, and profile variations with thickness. We illustrated our results and analyses using exponential $f_a(z)$ profile over the full range of values from $v_{af} = 99\%$ and $v_{fw} = 1\%$ and when we re-scaled it for any t from 0.2 cm to 10 cm, its shape remained the same. The available observations (section 2.4) suggest that this illustrative choice is reasonable. Yet, all three aspects of modeling $f_a(z)$ are debatable because they are based on insufficient information about void fraction profiles of natural sea foam under various conditions.

[69] For the shape, exponential variation in the foam layer thickness has not been observed directly; we inferred it from bubble-plume measurements and parameterizations (section 2.4). Meanwhile, directly observed shapes are for laboratory conditions with artificial foam and have not been parameterized. Thus, at present we cannot confidently recommend one profile shape over another.

[70] For the f_a range, it is quite possible that its upper and lower values v_{af} and v_{fw} each vary widely, leading to more variations of the e_f signal (section 4.2.3). An appropriate approach to represent v_{af} and v_{fw} could be the use of distributions, as *Reul and Chapron* [2003] proposed for sea foam thicknesses, rather than fixed values as we do to illustrate the results in this study. Of course, this approach raises

the question of the functional forms of such distributions, but no data currently exist to infer those.

[71] Finally, there is no definitive evidence for the preservation of either the f_a range or the shape of the profile when it is re-scaled for various t. Theoretically, an f_a profile from 99% to 1% (or any other range) can be spread over any t. But physical considerations suggest that in reality some combinations of t and f_a range might not be possible. Some foam thicknesses might necessarily be associated with narrower f_a ranges rather than with all possible f_a ranges; for instance, thin layers (e.g., $t \leq 0.5$ cm) with wet foam (e.g., $f_a \leq 60\%$, Figure 3). The reasoning behind this suggestion is that the thickness of a layer might restrict the number and sizes of the bubbles (e.g., *Deane and Stokes* [2002] among many) that can fit within the foam layer. Thin foam layers cannot hold large bubbles associated with dry foam and necessarily need to involve mostly small, thick-walled bubbles associated with wet foam (section 2.1). That is, foam layers with $t < 0.5$ cm might require $v_{af} \ll 99\%$. Connected to this suggestion is the possibility that for different f_a ranges different profile shapes are suitable, e.g., constant for very dry foam ($90\% < f_a < 99\%$), exponential for the transition from dry to wet foam ($60\% < f_a < 90\%$), and linear for wet foam ($1\% < f_a < 60\%$). *Raizer and Sharkov* [1982] used such an approach (section 2.4).

4.4.2. Modeling the Variations of Foam Emissivity

[72] The emissivity of a foam-covered surface e_f can vary widely for different frequencies F, foam layer thicknesses t, and ranges (from v_{af} to v_{fw}) of the void fraction profile $f_a(z)$ (section 4.2). With the concepts and understanding established in the previous sections, here we consider some aspects of modeling e_f and its variations.

[73] Figures 9b and 10 show that usually mechanically thin foam layers, i.e., $t < t_n(F)$, are also radiometrically thin with $t < d(F)$ and $Q_t(t) < d_s(F)$ (Table 3). If, however, pairing of thin layers with wet foam requires lower values for the upper limit v_{af} (section 4.4.1), then such layers might contain enough seawater so that $Q_t(t) > d_s(F)$ and $t > d(F)$. As a result, mechanically thin foam layers would be restricted to act mostly as radiometrically thick layers.

[74] Two modeling insights emerge from this reasoning. First, the microscopic characteristics of the sea foam (i.e., bubble sizes) impose the restriction described above, but it is expressed as a relationship between the foam macroscopic characteristics (t and f_a range) and foam dielectric properties (d and Q_t). This is useful knowledge when one weighs considerations of modeling foam emissivity in terms of a microscopic versus macroscopic set of variables.

[75] Second, we can use the nominal thicknesses t_n, identified for the full f_a range (Table 1), as markers to tune the upper limit of the f_a range to a lower value, excluding portions of the dry foam. For example, for a given combination of frequency F and foam thickness t, if $t < t_n(F)$ then the full f_a range should be reduced to a narrower range so that the condition for radiometrically thick layers $d < t$ holds true.

[76] While this may appear a reasonable modeling approach, as compared to the use of the full f_a range in all cases, we believe that its outcome could be flawed. Our arguments are the following. First, if we adjusted the f_a profile so that mechanically thin layers always emit as radiometrically thick layers, then we can expect little variations of e_f (Table 3) from

thin layers. This would contradict observations [*Bordonskiy et al.*, 1978] and models [*Guo et al.*, 2001; *Chen et al.*, 2003], which show variations of e_f for thin layers and saturation of e_f for thick layers. Only a system involving both radiometrically thin and radiometrically thick layers, with d varying around t, allows for wide e_f variations (Table 3 and section 4.2).

[77] Next, even if we decide to make such a tuning, we need to decide what values of v_{af} to use. Sections 2.4 and 4.4.1 show that, however scant, there is some experimental evidence for the full f_a range, while we know nothing about v_{af} values under open ocean conditions.

[78] Last, section 3.3 demonstrates that varying t alone invokes changes in d (thus e_f) as wide as varying the f_a range. We surmise, therefore, that at the current state of knowledge, fixing the void fraction limits to the full f_a range and exploring all possible t values could provide reasonable and encompassing simulations of the expected emissivity variations.

[79] Note, however, that all the considerations promoted here remain speculations until more observations under various conditions become available and corroborate or refute them.

4.5. Strong Absorption by Wet Foam

[80] In this section we use the foam skin depth results to gain insights about the contribution of different foam structures to the attenuation and emission of EM radiation.

[81] Since according to Kirchoff's law the emissivity of a medium at thermal equilibrium equals its absorptivity [*Peake*, 1959], to explain and model the medium emissivity, evaluation of its absorption losses is necessary. Based on the physical structure of sea foam (section 2.1), there are two possible mechanisms for absorption within foam layers, namely the seawater content and the dense packing of bubbles. Being conductive, seawater is the lossy constituent of the sea foam and its mere presence leads to absorption, which we call medium-intrinsic absorption. Densely packed bubbles cause multiple bounces of EM radiation on the bubble walls and lengthen the absorbing path. This enhances the medium-intrinsic absorption with additional absorption losses which we call scattering-driven absorption. The finding that scattering in foam is weak [*Anguelova*, 2008, section 2.3] implies that of these two pathways, the medium-intrinsic absorption is the major contributor to foam absorptivity.

[82] Fitting modeled foam emissivity to observations, *Webster et al.* [1976] found an optimal layer thickness of 0.15 ± 0.1 cm and explained this low (compared to observed thicknesses) value with the importance of the foam specific structure at the bottom of the foam layer. Saying "All the action is at the foam-water interface," Wilheit has always upheld this suggestion (T. T. Wilheit, International Geoscience and Remote Sensing Symposium, personal communication, 2006). Using our results for foam skin depth d, we can qualitatively illustrate Wilheit's conviction that the wet foam in the lower portion of a foam layer suffices for strong absorption in and emission by foam while the dry foam in the upper part of the foam layer contributes little. Note that the dry foam does play an important role for the high foam absorptivity, but rather than absorbing the EM radiation directly, it transmits the radiation effectively to the absorbing component. These aspects of the sea foam dielectric properties will be detailed in AG11.

[83] Because the foam dielectric constant ε_f does not include scattering losses (section 2.3), the attenuation coefficient α in equations (1a), (1b), (2a), and (2b) represents the medium-intrinsic, purely absorption losses. Therefore, we can consider the calculated d to be a measure of the absorption strength of the medium itself: the thinner the skin depth, the stronger the absorption.

[84] According to Figure 3, at 10.7 GHz and a void fraction of 95%, foam as thick as 173 cm would be necessary in order to register 86% of the signal from it, seawater below excluded. The need for such thick skin depth indicates that the intrinsic absorption of dry foam is negligible. Meanwhile, d of layers comprising wet foam (e.g., with f_a up to about 60%) differ from d_s by at most a factor of 3.5 (recall section 3.2). Therefore, we can state that the medium-intrinsic absorption of wet foam is on the same order as that of seawater. The variations of d observed when wet and dry foam contribute differently to the void fraction profile in a foam layer (Figures 8 and 10) reinforce this conclusion.

[85] In short, the water-laden, wet foam close to the foam-water boundary is the major contributor to the high absorptivity of a foam layer.

5. Conclusions

[86] Investigation of foam skin depth d in vertically structured foam layers for frequencies F from 1 to 37 GHz is presented for the first time. Various void fraction profiles $f_a(z)$ can represent the variations of foam mechanical structure within the foam thickness t. The complex permittivity of sea foam $\varepsilon_f(z)$ resulting from a void fraction $f_a(z)$ profile (section 2.4) is used to calculate d for various t covering the range of thicknesses encountered in the ocean (section 2.5). The physical insights of this study are as follows:

[87] 1. The foam skin depth d obtained with exponential $f_a(z)$ profile from 99% to 1% varies from 0.17 cm to no more than 7 cm for foam thicknesses from 0.2 cm to 10 cm (Figure 4, Table 1, and section 2.4).

[88] 2. The frequency dependence of foam skin depth $d(F)$ varies with the choice of the mixing rule for $\varepsilon_f(z)$ (Figure 5); seawater temperature and salinity (Figure 6); shape of $f_a(z)$ as well as its range from upper to lower limits (Figures 7 and 8). Varied t and f_a range lead to the widest variations of $d(F)$.

[89] 3. The requirement to distinguish foam from the surrounding seawater using passive microwave remote sensing is foam skin depth larger than the seawater skin depth $d > d_s$ (section 4.1.1). This requirement is breached for thin foam layers (<0.5 cm) at low frequencies. The remote sensing implication of this finding is that low frequencies cannot probe whitecaps created under low wind speed conditions or residual foam.

[90] 4. Depending on the relationships among d, t, and the f_a range, the thermal emission from foam layers could be from the entire foam layer, from part of the foam layer, or from both the foam layer and seawater. Each case results in characteristic variations of the foam emissivity (section 4.2, Table 3, and Figure 10).

[91] 5. The interplay between d, t, and the f_a range provides a basis for frequency sensitivity to foam thickness, which is the reason that different frequencies measure the same sea state involving foam differently (section 4.2.2).

This has implications for the passive microwave remote sensing of oceanic whitecaps (section 4.3).

[92] 6. The results for d illustrate that the wet portion of the vertically structured foam layer is the main contributor to the medium-intrinsic absorption losses in foam (section 4.5).

[93] The conclusions of this study on the possible approaches to model foam emissivity of vertically structured foam layers are as follows:

[94] 1. Lack of experimental observations is currently the main reason for uncertainties in choosing approaches and parameters to model vertically stratified foam with a void fraction profile (section 4.4.1).

[95] 2. The shape and the seawater content of the void fraction profile $f_a(z)$ can be controlled either with the choice of the functional formulation of f_a or with profile parameters (Table 2 and sections 3.1 and 4.4.1).

[96] 3. Using a range of foam thicknesses t in combination with a void fraction profile covering the full f_a range could be an acceptable modeling approach until more information about f_a and its relation to t becomes available (section 4.4).

[97] Having a more complete physical understanding of the foam dielectric constant [Anguelova, 2008] and foam skin depth (present study), in AG11 we will consider the foam dielectric properties responsible for the propagation of EM radiation through foam. The combination of these various analyses will provide a conceptual understanding of the high, blackbody-like emissivity of sea foam.

References

Andreas, E. L., P. P. G. Persson, and J. E. Hare (2008), A bulk turbulent air-sea flux algorithm for high-wind, spray conditions, *J. Phys. Oceanogr.*, *38*, 1581–1596, doi:10.1175/2007JPO3813.1.

Anguelova, M. D. (2008), Complex dielectric constant of sea foam at microwave frequencies, *J. Geophys. Res.*, *113*, C08001, doi:10.1029/2007JC004212.

Anguelova, M. D., and F. Webster (2006), Whitecap coverage from satellite measurements: A first step toward modeling the variability of oceanic whitecaps, *J. Geophys. Res.*, *111*, C03017, doi:10.1029/2005JC003158.

Atkinson, K. A. (1989), *An Introduction to Numerical Analysis*, 2nd ed., 712 pp., John Wiley, New York.

Bikerman, J. J. (1953), *Foams: Theory and Industrial Applications*, pp. 347, Reinhold, New York.

Blenkinsopp, C. E., and J. R. Chaplin (2007), Void fraction measurements in breaking waves, *Proc. R. Soc. A*, *463*, 3151–3170, doi:10.1098/rspa.2007.1901.

Bordonskiy, G. S., et al. (1978), Spectral characteristics of the emissivity of foam formations, *Izv. Russ. Acad. Sci. Atmos. Oceanic Phys., Engl. Transl.*, *14*, 464–469.

Camps, A., et al. (2005), The emissivity of foam-covered water surface at L-band: Theoretical modeling and experimental results from the FROG 2003 field experiment, *IEEE Trans. Geosci. Remote Sens.*, *43*, 925–937, doi:10.1109/TGRS.2004.839651.

Chen, D., L. Tsang, L. Zhou, S.C. Reising, W.E. Asher, L.A. Rose, K.-H. Ding, and C.-Te Chen (2003), Microwave emission and scattering of foam based on Monte Carlo simulations of dense media, *IEEE Trans. Geosci. Remote Sens.*, *41*, 782–790, doi:10.1109/TGRS.2003.810711.

Dahl, P., and A. Jessup (1995), On bubble clouds produced by breaking waves: An event analysis of ocean acoustic measurements, *J. Geophys. Res.*, *100*, 5007–5020, doi:10.1029/94JC03019.

Deane, G. B., and M. D. Stokes (2002), Scale dependence of bubble creation mechanisms in breaking waves, *Nature*, *418*, 839–844, doi:10.1038/nature00967.

de Leeuw, G., E. L. Andreas, M. D. Anguelova, C. W. Fairall, E. R. Lewis, C. D. O'Dowd, M. Schulz, and S. E. Schwartz (2011), Production flux of sea spray aerosol, *Rev. Geophys.*, *49*, RG2001, doi:10.1029/2010RG000349.

Droppleman, J. (1970), Apparent microwave emissivity of sea foam, *J. Geophys. Res.*, *75*, 696–698, doi:10.1029/JC075i003p00696.

Gemmrich, J. R., and D. M. Farmer (1999), Observations of the scale and occurrence of breaking surface waves, *J. Phys. Oceanogr.*, *29*, 2595–2606, doi:10.1175/1520-0485(1999)029<2595:OOTSAO>2.0.CO;2.

Gordon, H. R., and M. Wang (1994), Influence of oceanic whitecaps on atmospheric correction of ocean-color sensors, *Appl. Opt.*, *33*(33), 7754–7763, doi:10.1364/AO.33.007754.

Guo, J., L. Tsang, W. Asher, K.-H. Ding, and C.-T. Chen (2001), Applications of dense media radiative transfer theory for passive microwave remote sensing of foam covered ocean, *IEEE Trans. Geosci. Remote Sens.*, *39*, 1019–1027, doi:10.1109/36.921420.

Kolovayev, P. A. (1976), Investigation and statistical size distribution of wind produced bubbles in the near-surface ocean layer, *Oceanology, Engl. Transl.*, *15*, 659–661.

Lamarre, E., and W. K. Melville (1991), Air entrainment and dissipation in breaking waves, *Nature*, *351*, 469–472, doi:10.1038/351469a0.

Leifer, I., and G. de Leeuw (2006), Bubbles generated from wind-steepened breaking waves: 1. Bubble plume bubbles, *J. Geophys. Res.*, *111*, C06020, doi:10.1029/2004JC002673.

Leifer, I., G. Caulliez, and G. de Leeuw (2006), Bubbles generated from wind-steepened breaking waves: 2. Bubble plumes, bubbles, and wave characteristics, *J. Geophys. Res.*, *111*, C06021, doi:10.1029/2004JC002676.

Maul, G. A. (1985), *Introduction to Satellite Oceanography*, 606 pp., Martinus Nijhoff, Boston, Mass.

Melville, W., E. Terrill, and L. Ding (1995), Field measurements of air entrainment by breaking waves, in *Air-Water Gas Transfer*, edited by B. Jähne and E. Monahan, pp. 285–295, Verlag and Studio, Hanau, Germany.

Militskii, Y. A., V. Y. Raizer, E. A. Sharkov, and V. S. Etkin (1977), Scattering of microwave radiation by foamy structures, *Radio Eng. Electron. Phys., Engl. Transl.*, *22*, 46–50.

Padmanabhan, S., S. C. Reising, W. E. Asher, L. A. Rose, and P. W. Gaiser (2006), Effects of foam on ocean surface microwave emission inferred from radiometric observations of reproducible breaking waves, *IEEE Trans. Geosci. Remote Sens.*, *44*, 569–583, doi:10.1109/TGRS.2006.870234.

Pandey, P., and R. Kakar (1982), An empirical microwave emissivity model for a foam-covered sea, *IEEE J. Oceanic Eng.*, *7*, 135–140, doi:10.1109/JOE.1982.1145527.

Peake, W. (1959), Interaction of electromagnetic waves with some natural surfaces, *IRE Trans. Antennas Propag.*, *7*, suppl., 324–329, doi:10.1109/TAP.1959.1144736.

Peltzer, R. D., and O. M. Griffin (1987), Stability and decay properties of foam in seawater, *NRL Memo. Rep.*, *5949*, 59.

Peltzer, R. D., and O. M. Griffin (1988), Stability of a three-dimensional foam layer in seawater, *J. Geophys. Res.*, *93*, 10,804–10,812, doi:10.1029/JC093iC09p10804.

Raizer, V. (2007), Macroscopic foam-spray models for ocean microwave radiometry, *IEEE Trans. Geosci. Remote Sens.*, *45*, 3138–3144, doi:10.1109/TGRS.2007.895981.

Raizer, V. Y., and E. A. Sharkov (1982), Electrodynamic description of densely packed dispersed systems, *Radiophys. Quantum Electron.*, Engl. Transl., *24*, 553–560.

Reising, S. C., W. E. Asher, and L. A. Rose (2002), Polarimetric emissivity of whitecaps experiment (POEWEX): Preliminary results, paper presented at WindSat Science Workshop, Noesis, Inc., Arlington, Va., Nov.

Reul, N., and B. Chapron (2003), A model of sea-foam thickness distribution for passive microwave remote sensing applications, *J. Geophys. Res.*, *108*(C10), 3321, doi:10.1029/2003JC001887.

Rose, L. A., W. E. Asher, S. C. Reising, P. W. Gaiser, K. M. St Germain, D. J. Dowgiallo, K. A. Horgan, G. Farquharson, and E. J. Knapp (2002), Radiometric measurements of the microwave emissivity of foam, *IEEE Trans. Geosci. Remote Sens.*, *40*, 2619–2625, doi:10.1109/TGRS.2002.807006.

Ryu, Y., and K. Chang (2008), Green water void fraction due to breaking wave impinging and overtopping, *Exp. Fluids*, *45*, 883–898, doi:10.1007/s00348-008-0507-3.

Sihvola, A. (1999), *Electromagnetic Mixing Formulas and Applications*, 284 pp., Inst. of Electr. Eng., London.

Stogryn, A. P. (1997), Equations for the permittivity of sea water, report to Naval Research Laboratory, 11 pp., GenCorp Aerojet, Azusa, Calif.

Thorpe, S. (1982), On the clouds of bubbles formed by breaking wind-waves in deep water, and their role in air-sea gas transfer, *Philos. Trans. R. Soc. London A*, *304*, 155–210, doi:10.1098/rsta.1982.0011.

Ulaby, F., R. Moore, and A. Fung (1982), *Microwave Remote Sensing: Active and Passive, From Theory to Applications*, vol. II, 2162 pp., Book-Mart, North Bergen, N. J.

Ulaby, F., R. Moore, and A. Fung (1986), *Microwave Remote Sensing: Active and Passive, From Theory to Applications*, vol. III, 2162 pp., Book-Mart, North Bergen, N. J.

Walsh, A., and P. Mulhearn (1987), Photographic measurements of bubble population from breaking waves at sea, *J. Geophys. Res.*, *92*, 14,553–14,565, doi:10.1029/JC092iC13p14553.

Wanninkhof, R., W. E. Asher, D. T. Ho, C. Sweeney, and W. R. McGillis (2009), Advances in quantifying air-sea gas exchange and environmental forcing, *Annu. Rev. Mater. Sci.*, *1*, 213–244, doi:10.1146/annurev.marine.010908.163742.

Webster, W. J., T. T. Wilheit, D. B. Ross, and P. Gloersen (1976), Spectral chacteristics of the microwave emission from a wind-driven foam-covered sea, *J. Geophys. Res.*, *81*, 3095–3099, doi:10.1029/JC081i018p03095.

Wentz, F. (1983), A model function for ocean microwave brightness temperature, *J. Geophys. Res.*, *88*, 1892–1908, doi:10.1029/JC088iC03p01892.

Wilheit, T. T. (1978a), Radiative transfer in a plane stratified dielectric, *IEEE Trans. Geosci. Electron.*, *16*, 138–143, doi:10.1109/TGE.1978.294577.

Wilheit, T. T. (1978b), A review of applications of microwave radiometry to oceanography, *Boundary Layer Meteorol.*, *13*, 277–293, doi:10.1007/BF00913878.

Wilheit, T. T. (1979), A model for the microwave emissivity of the ocean's surface as a function of wind speed, *IEEE Trans. Geosci. Electron.*, *17*, 244–249, doi:10.1109/TGE.1979.294653.

Williams, G. F. (1971), Microwave emissivity measurements of bubbles and foam, *IEEE Trans. Geosci. Electron.*, *9*, 221–224, doi:10.1109/TGE.1971.271504.

Wu, J. (1994), Bubbles in the near-shore ocean: Their various structures, *J. Phys. Oceanogr.*, *24*, 1955–1965, doi:10.1175/1520-0485(1994)024<1955:BITNSO>2.0.CO;2.

Yueh, S. (1997), Modeling of Wind Direction Signals in Polarimetric Sea Surface Brightness Temperatures, *IEEE Trans. Geosci. Remote Sens.*, *35*, 1400–1418, doi:10.1109/36.649793.

M. D. Anguelova and P. W. Gaiser, Remote Sensing Division, Naval Research Laboratory, Code 7223, 4555 Overlook Ave., SW, Washington, DC 20375, USA. (maggie.anguelova@nrl.navy.mil)